PLSTM-Reg v1.0: A regional physics-encoded LSTM model for simulating reservoir operations under data scarcity

Bin Yu[1], Yanan Chen[1], Yi Zheng[123]*

[1] School of Environmental Science and Engineering, Southern University of Science and Technology, Shenzhen, China

[2] School of Engineering, Westlake University; Hangzhou 310030, Zhejiang Province, ChinaShenzhen Municipal Engineering Lab of Environmental IoT Technologies, Southern University of Science and Technology, Shenzhen, China

[3] State Environmental Protection Key Laboratory of Integrated Surface Water - Groundwater Pollution Control, Southern University of Science and Technology, Shenzhen, China

* *Correspondence to*: Yi Zheng (zhengy@sustech.edu.cn)

Abstract. Representing reservoir operations in large-scale hydrological models remains difficult due to complex release decisions and scarce operational records. Here, we develop PLSTM-Reg v1.0, a regional physics-encoded deep learning framework that explicitly enforces mass balance and operational constraints to simulate reservoir operations across diverse systems. The framework is evaluated using 256 representative reservoirs across the Contiguous United States, focusing on three core capabilities: temporal generalization to unseen periods, spatial transfer to unseen reservoirs, and historical data reconstruction in data-scarce reservoirs. Under temporal testing, the regional model improves 1-day-ahead release forecasts from a median Kling–Gupta Efficiency (KGE) of 0.83 to 0.96 relative to local counterparts (i.e., models trained exclusively on site-specific records), and reduces poorly simulated cases (KGE < 0.8) from 41.8% to 2.3%. For long-term simulation, storage performance reaches a median KGE of 0.79, a modest gain over local models (0.76) but with notable robustness for reservoirs with large capacity. When transferred to unseen reservoirs, the model substantially outperforms widely used rule-based schemes: median KGE rises from 0.55 (best benchmark) to 0.73 for release and from 0.22 to 0.59 for storage, and the proportion of usable simulations (KGE > 0.5) increases from 56.6% to 89.8% for release and 14.4% to 61.7% for storage. In historical storage reconstruction, incorporating monthly satellite-derived surface area as a proxy for missing ground-based records enables reconstruction accuracy comparable to local models. These results demonstrate that cross-reservoir deep learning combined with physical knowledge provides a scalable scheme for representing human water

management within large-scale hydrological and land surface models under widespread data scarcity.

1 Introduction

Approximately 2.8 million dams exist globally (Grill et al., 2019), including over 90,000 in the United States (DeNeale et al., 2019). Reservoirs sustain societies through flood control, water supply, and hydropower (Haemmerli et al., 2024; Zhao et al., 2020), while profoundly altering water cycles (Chalise et al., 2021; Fan et al., 2024). However, hydrological and land surface models struggle to represent their operations due to complex human decision-making (Longyang and Zeng, 2023; Turner et al., 2020) and scarce publicly available operational records (Steyaert and Condon, 2024), creating substantial biases in large-scale water resource assessments (Li et al., 2025; Turner et al., 2020, 2021). Although large-scale models such as PCR-GLOBWB (Sutanudjaja et al., 2018) and the NOAA National Water Model (Cosgrove et al., 2024) incorporate simplified regulation schemes (Hanasaki et al., 2008a; Shen et al., 2025; Wisser et al., 2010; Zajac et al., 2017), they remain unable to realistically reproduce observed flows (Steyaert and Condon, 2024; Vora et al., 2024). Scalable approaches for data-scarce reservoirs are thus urgently needed to improve the representation of human-water interactions in these large-scale models.

Rule-based reservoir operation models (Hanasaki et al., 2008a, b; Wisser et al., 2010; Zajac et al., 2017) are widely used in large-scale hydrological studies because of their interpretability and modest data requirements. However, their fixed recommended parameters and simplified operating rules limit their ability to represent site-specific and nonlinear real-world operating behavior (Steyaert and Condon, 2024; Yang et al., 2021). Some progress has been made in recent studies. Yassin et al. (2019) proposed an improved target storage-and-release parameterization that better represents reservoir storage zones and seasonal release behavior, but it requires in-situ storage and release series (or distributions) to determine model parameters. Turner et al. (2021) developed a transferable rule-based framework that learns operating policies from data-rich reservoirs and extrapolates them to neighboring data-scarce reservoirs with similar purposes. However, directly transferring the same policy parameters from source reservoirs to target reservoirs may impose source-specific operating behavior and introduce significant bias.

Recently, machine learning has been introduced to improve the parameterization and transferability of rule-based reservoir operation schemes. Some studies have used machine learning to estimate parameters for existing operation schemes, such as reservoir-operation parameters inferred from reservoir attributes using Random Forest models (Steyaert et al., 2025) and flood storage capacities estimated using XGBoost to define storage-zone parameters in a target storage scheme (Shen et al., 2025). Researchers have also explored the use of machine learning to develop hybrid models for improved reservoir representation. Chen et al. (2022) developed a data-driven framework that extracts interpretable operation modules and associated application conditions from historical operation records. Building on this modular reservoir modeling concept, Li and Villarini (2026) further investigated its generalization using Random Forest models to transfer parameters associated with typical operation modules, such as constant, linear, and piecewise-linear release relationships, across reservoirs. Although these approaches improve parameter estimation and transferability while retaining interpretability, they generally represent reservoir operations through simplified modules or predefined rules. Moreover, because these modules or parameters are typically identified from individual reservoirs before being transferred, these approaches cannot fully leverage cross-site information during model training, which has been shown to improve the generalization of regional deep learning models (Fang et al., 2022; Kratzert et al., 2024). Consequently, their ability to learn complex operating behavior across diverse reservoirs may remain constrained.

Another line of research uses machine learning directly for reservoir operation modeling in an end-to-end way. Site-specific models based on decision trees (Dong et al., 2023a; Yang et al., 2016, 2021), recurrent neural networks (Cheng et al., 2024; Yang et al., 2019), LSTM variants (Longyang and Zeng, 2023; Zhang et al., 2018), and physics-encoded deep learning (Yu et al., 2025; Zheng et al., 2022) have shown strong ability to learn release behavior directly from historical records without prescribing explicit operating rules. However, these models require local operational data for training and therefore have limited applicability to data-scarce reservoirs. To address this limitation, recent studies have begun to explore regional end-to-end models that learn release behavior across multiple reservoirs. Ford and Sankarasubramanian (2023) proposed a regionalized piecewise linear regression tree framework for reservoir release prediction, but its reliance on reservoir-specific release and storage statistics for normalization limits direct transfer to unseen reservoirs without historical operation records. Tran et al. (2025) developed a

conditioned LSTM for daily reservoir release prediction across CONUS reservoirs using static reservoir attributes, demonstrating the potential of pooled deep learning for reservoir operations. However, the model focuses on next-day release prediction, relies on observed storage as an input, and does not explicitly enforce mass balance. In contrast, long-term reservoir simulation requires the model to internally evolve storage states while maintaining mass balance, which remains largely unexplored.

This study aims to leverage knowledge learned across many reservoirs to address the longstanding challenge of simulating reservoir operations under data scarcity. Here "data scarcity" specifically refers to the lack of historical operational records required for site-specific training or calibration, rather than the absence of hydrological forcing. We develop PLSTM-Reg v1.0, a regional physics-encoded LSTM framework designed to emulate human decision-making in reservoir operations. A dataset of 256 representative reservoirs across the Contiguous United States (CONUS), each with multi-decadal daily inflow, release, and storage records, provides the basis for evaluation. The framework is examined with respect to three central expectations. The first concerns temporal generalization, testing whether regional training improves predictive skill during unseen periods relative to models trained solely on local records. The second addresses spatial generalization, determining whether the regional model can be reliably transferred to data-scarce reservoirs and outperform widely used rule-based schemes. The third investigates historical reconstruction in data-scarce reservoirs, evaluating the regional model's ability to recover past reservoir behavior, particularly storage dynamics, using readily available remote-sensing data. Together, these assessments provide a systematic evaluation of whether shared learning across reservoirs can enhance reservoir simulation and offer a scalable pathway for representing human water management in large-scale hydrological modeling.

2 Data and methods

2.1 Data

This study evaluated 256 major reservoirs across the CONUS (Fig. 1), with daily inflow, release, and storage observations obtained from Chen et al. (2025). Notably, the dataset provides net inflow derived from the observed storage–release balance ($I_{net,t} = S_{t+1} - S_t + R_t$), providing an internally closed water balance formulation that implicitly incorporates unobserved

fluxes such as evaporation and seepage. The reservoirs were selected based on record availability and data quality, requiring at least 25 years of continuous records spanning 1990–2021 (end dates ranged from 31 December 2014 to 30 April 2021) and <10% missing data. To characterize upstream hydrologic conditions, catchment boundaries were delineated using MERIT-Hydro and MERIT-Basins (Lin et al., 2019; Yamazaki et al., 2019) through the "delineator" package (Heberger, 2023). Resulting catchment areas were validated against reported values in the Global Dam Watch (GDW) database (Lehner et al., 2024), and delineations were manually corrected when relative error exceeded 10%. Catchment-scale forcings, including daily mean temperature and total precipitation, were obtained from the Daymet dataset (Thornton et al., 2022, 2021) and spatially averaged over each delineated catchment. These forcings complement the reservoir-specific dynamic inputs (daily inflow and storage) used in the modeling framework.

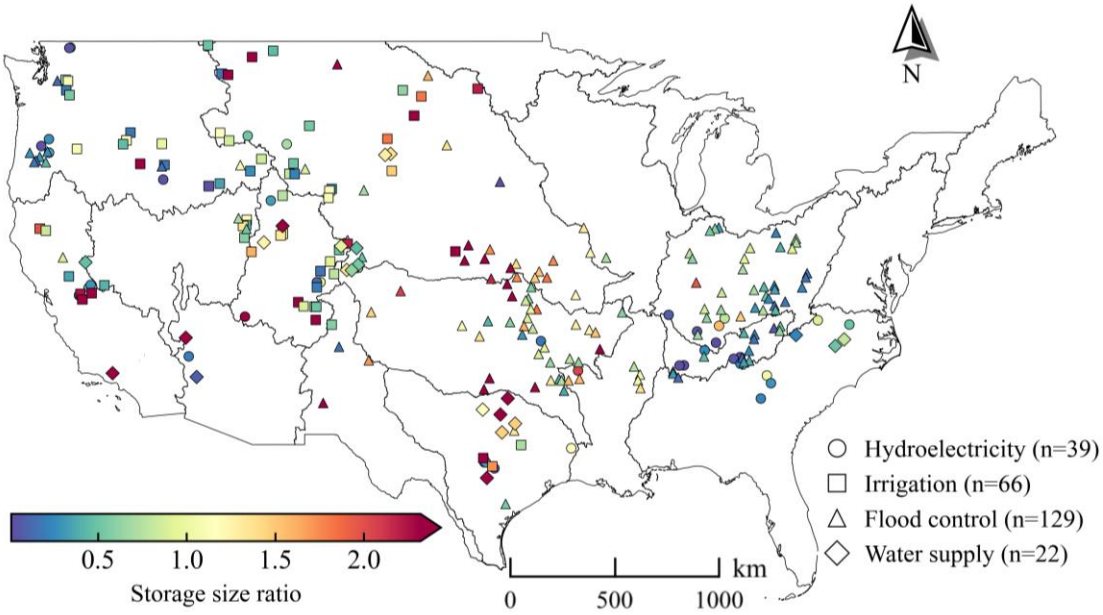


Figure 1. Spatial distribution of the 256 reservoirs across the CONUS. Each marker denotes a reservoir, with marker shape indicating the primary operational purpose and color representing the storage size ratio. This map highlights the geographic breadth and functional diversity of the reservoir network used for model training and evaluation.

For each reservoir, we compiled static attributes from the GDW database, including physical characteristics (e.g., dam height, storage capacity), primary management purpose, and hydrological context (i.e., long-term mean discharge at the dam location during 1971–2000). We also derived the catchment-scale static attributes: mean annual precipitation and temperature from Daymet, and the aridity index from the Global Aridity Index dataset (Zomer et al., 2022). In total,

21 static attributes were compiled (Table A1). These attributes highlight the diversity of the 256 reservoirs. Storage capacities span 0.1–31.2 km³, and storage size ratios (i.e., storage capacity divided by mean annual inflow) range from 0.01 to 11.41, encompassing from small, near-natural reservoirs to large, heavily regulated ones. Management purposes are distributed across flood control (129), irrigation (66), hydroelectric generation (39), and water supply (22). The reservoirs span 15 of the 18 HUC2 water regions across the CONUS, demonstrating broad geographic and hydroclimatic representativeness. Their spatial distribution and key attributes (primary purpose and storage size ratio) are shown in Fig. 1.

In addition, to evaluate the contribution of remote sensing data to reconstructing operation records (specifically storage and release) for data-scarce reservoirs, we incorporated monthly satellite-derived surface area time series from the Global Reservoir Surface Area Dataset (GRSAD; Zhao and Gao, 2018), which provides data for 6,817 reservoirs listed in the GRanD database from 1984 to 2018. Prior to imputation, the raw monthly GRSAD time series across the evaluated reservoirs had an average missing-data ratio of 3.7%, with reservoir-level values ranging from 0% to 6.6%. For missing values within the GRSAD record, data were imputed according to gap length: gaps of six months or shorter were linearly interpolated, whereas longer gaps were filled with the long-term monthly mean surface area. For periods extending beyond the GRSAD coverage (post-2018), the same climatological monthly mean was used to maintain dataset consistency and avoid cross-product biases.

2.2 Model architecture

This study introduces PLSTM-Reg v1.0, a regional Physics-Encoded LSTM (PLSTM) framework (Fig. 2a) for reservoir operation modeling. The model processes two categories of inputs I_t: dynamic forcings (precipitation, mean temperature, inflow, storage, and day of the year) and static attributes (Table A1). Although explicit water-demand data are not used, demand-related operational patterns may be implicitly represented through the model inputs. Seasonal indicators, hydrometeorological forcings, and static attributes such as reservoir purpose provide information related to the timing and magnitude of water demands. Furthermore, historical storage and release records reflect the cumulative effects of reservoir operation decisions driven by water demands and management objectives, thereby providing indirect information on demand-related operating behaviors. Each input group is first transformed through a dedicated embedding network (a two-

layer fully connected neural network, FCNN) to extract dynamic features and static site-specific condition vectors. The resulting embedding streams are concatenated into a combined input vector x_t, which is passed to the core PLSTM layer adopting the physics-encoded architecture of Yu et al. (2025).

Unlike a standard LSTM, which maintains an abstract cell state c_t, the PLSTM introduces a physically meaningful internal state s_t that directly tracks reservoir storage. Within this layer (Fig. 2b), the recurrent unit generates hidden states h_t, which are mapped through a fully connected output layer to produce candidate predictions $\tilde{r}_t$. These candidates are then processed by a physical constraint module that enforces mass conservation and valid bounds on release and storage. Note that while the architecture supports operational release bounds (Eq. S8), this constraint is not activated in this study because reservoir-specific release limits are unavailable for the large-sample reservoir dataset. At each timestep, the updated simulated storage state s_t is propagated recurrently to the subsequent PLSTM cell and concatenated internally with the recurrent state h_t, as well as external input vector x_t (Fig. 2b). As s_t is generated by the model rather than externally prescribed, it is not treated as a dynamic input. This architecture provides an endogenous mechanism for maintaining physically feasible behavior and mitigating ~~ensures physically feasible behavior and prevents~~ long-term mass-balance drift, as demonstrated in Yu et al. (2025)~~.~~. Because the simulated storage state influences the subsequent release prediction, a deviation in storage can induce corresponding changes in simulated release that may counteract further error accumulation. For example, an overestimated storage state may lead the model to predict a larger release, which in turn reduces the storage estimate at the next timestep.

It is worth noting that although hard physical bounds implemented via the torch.clamp function may truncate gradients when constraints are exceeded, preliminary experiments showed stable optimization without requiring smoothing techniques (e.g., tanh smoothing). Similar implementations are also adopted in recent differentiable hydrology frameworks such as hydrodl2 (mhpi, 2026). Full mathematical details are provided in Supplementary Text S1. For comparison, we also implemented local PLSTM models (PLSTM-Loc) trained separately for each reservoir to assess the value of regional information. Following Kratzert et al. (2024), the local models adopt a simplified architecture to reduce overfitting risks. The network dimensions for both model configurations are summarized in Table S1.

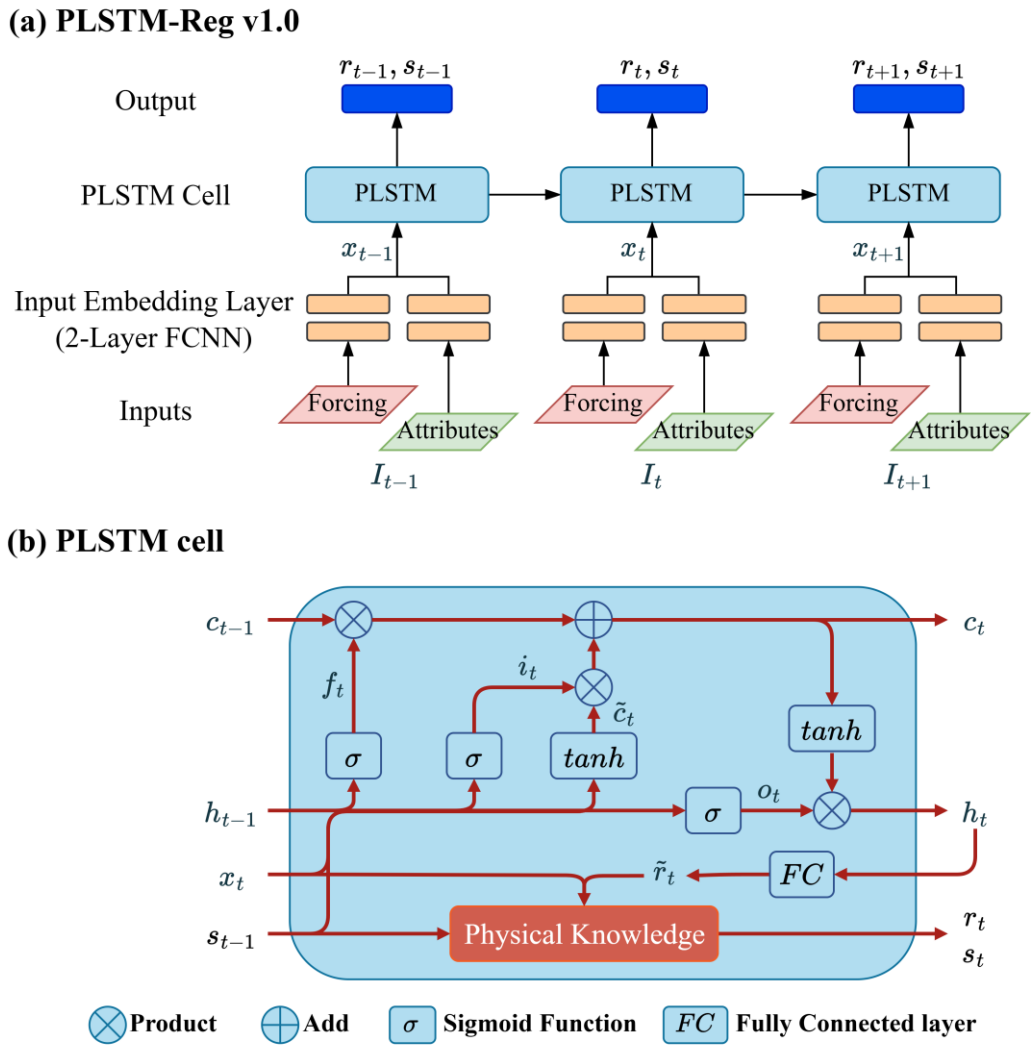


Figure 2. The PLSTM-Reg v1.0 model. (a) Model architecture. Dynamic forcings and static attributes are processed by separate embedding networks (two-layer FCNNs) and fused into the input vector x_t. (b) PLSTM cell. The cell introduces an explicit storage state s_t alongside the standard LSTM states c_t and h_t. The "Physical Knowledge" module (red box) enforces mass balance and physical bounds on the candidate release $\tilde{r}_t$, producing physically consistent release r_t and storage s_t outputs.

All models were implemented using the NeuralHydrology package (Kratzert et al., 2022), which is built on the PyTorch framework (Paszke et al., 2019). Before model training, storage, release, and inflow were first normalized by the storage capacity of each reservoir. These capacity-normalized variables were then standardized ~~Data normalization was performed~~ using regional scaling factors computed from the training set, rather than per-reservoir statistics. The physical storage constraint is applied after reversing the regional standardization but without reversing the capacity normalization, such that the bound [0,1] corresponds to $0 \leq S_t \leq S_{capacity}$ for each

reservoir. Model optimization was performed with the Adam algorithm (Kingma and Ba, 2015) to minimize the Nash–Sutcliffe Efficiency (NSE; Nash and Sutcliffe, 1970) loss. Regional models were trained for up to 20 epochs with a batch size of 512, while local models were trained for up to 100 epochs with a batch size of 256. To assess modeling uncertainty, each model was trained ten times using different random seeds. For each reservoir, data were split chronologically into training (1990–2004), validation (2005–2009), and testing (2010 onward) periods. The testing period extends to the end of each site's available record, ensuring at least five years of data.

2.3 Experimental design and model evaluation

The proposed regional DL framework was evaluated for temporal and spatial generalization: performance on unseen periods at data-rich reservoirs and on unseen reservoirs in data-scarce contexts. Two real-world application scenarios, short-term prediction (lead times <= 7 days) and long-term simulation, were tested under both temporal and spatial generalization settings. Specifically, short-term prediction (Experiments I and III) supports real-time operational decision-making, where storage observations are typically available, while long-term simulation (Experiments II and IV) is designed for coupling with Large-scale Hydrological Models (LHMs) to assess future climate change impacts, where operational records do not exist. In addition, we explored the potential of using satellite data to recover historical records for data-scarce regions via our regional models (Experiment V). To support these analyses, we designed five numerical experiments (Experiments I–V), summarized in Table 1 and described in detail later in this section.

Table 1. Five numerical experiments and corresponding model configurations.

ID	Modeling scheme	Generalization type	Dynamic inputs
I	Short-term prediction	Temporal (Chronological Split)	P, T, DoY, Inflow, Storage
II	Long-term simulation	Temporal (Chronological Split)	P, T, DoY, Inflow
III	Short-term prediction	Spatial (Cross-Validation)	P, T, DoY, Inflow, Storage
IV	Long-term simulation	Spatial (Cross-Validation)	P, T, DoY, Inflow
V	Historical reconstruction	Spatial (Cross-Validation)	P, T, DoY, Inflow, RS

Notes: P (precipitation), T (temperature), DoY (day of year), and RS (remote-sensing-derived monthly surface area).

Experiments I and II evaluate whether regional learning enhances predictive skill for data-rich reservoirs using a chronological split. In short-term prediction (Experiment I), PLSTM models were trained in a sequence-to-one manner with a sequence length of 180 days to predict next-day release and storage. For lead times beyond one day, the model is run recursively, using the predicted storage from the previous step as input. This structure follows standard hydrological prediction practice (Dong et al., 2023a; Kratzert et al., 2019) and is required because the model uses storage at day t to predict release and storage at day t+1. In long-term simulation (Experiment II), we tested the models' ability to maintain physical consistency over multi-year reservoir operation using a sequence-to-sequence configuration. The sequence length for both model training and testing was set to 1460 days (4 years). A sensitivity analysis using 2-, 4-, and 6-year sequence lengths yielded similar performance across all tested settings (Supplementary Fig. S1), indicating that the results are not strongly sensitive to this choice. In this configuration, only the initial storage is prescribed, and the model simulates storage forward in time based solely on its internal dynamics and the mass-balance and range constraints embedded in the PLSTM cell. In both experiments, we benchmarked our regional models (PLSTM-Reg) against local counterparts (PLSTM-Loc) to quantify the added value of incorporating regional information. In Experiment II, we also compared PLSTM-Reg with the calibrated ISTARF model (Turner et al., 2021), using parameters fitted from the training period of each reservoir and evaluated on the chronological test period. The implementation details are provided in Supplementary Text S2.

Experiments III and IV evaluate the model's spatial generalizability to data-scarce reservoirs, under both short-term prediction (Experiment III) and long-term simulation (Experiment IV) settings. We adopted a five-fold spatial cross-validation protocol (Feng et al., 2021; Kratzert et al., 2019) to assess performance on held-out reservoirs. We further benchmarked the regional model against four widely used rule-based schemes: the HANA model (Hanasaki et al., 2008a), the WISS model (Wisser et al., 2010), the ZAJC model (Zajac et al., 2017), and the transferred ISTARF model (Turner et al., 2021). To ensure a fair comparison, each benchmark was implemented with its recommended parameters (details in Supplementary Text S2). Furthermore, for all simulations in data-scarce settings (Experiment IV and benchmarks), storage was initialized at 50% of reservoir capacity, whereas observed initial storage was used during training. A 1-year warm-up period was applied to equilibrate model states. Sensitivity analysis

confirming the robustness of the model to this initial storage assumption is provided in Supplementary Fig. S2.

Experiment V further investigates the value of satellite-derived information for reconstructing historical records in data-scarce reservoirs using PLSTM-Reg. In this configuration (PLSTM-Reg+RS), the regional model takes monthly surface-area time series from GRSAD as an additional input. To align with the model's daily temporal resolution, monthly surface area values were assigned to the midpoint of each month and linearly interpolated to daily time steps. The interpolated daily series may use within-month information from both earlier and later dates, which is appropriate for the reconstruction setting because the complete historical surface-area record is available during reconstruction. Because water surface area reflects underlying storage dynamics, we hypothesize that incorporating widely available remote-sensing observations can guide the learning process and improve daily-scale storage estimates.

Model performance was evaluated using several widely adopted statistical metrics. Our primary metric is the Kling–Gupta Efficiency (KGE; Gupta et al., 2009), which provides a holistic assessment by decomposing model skill into correlation, bias, and variability components. We also report the NSE and the Pearson Correlation Coefficient (Corr), both widely used for evaluating hydrological simulations. These metrics are defined as:

$$\mathrm{KGE} = 1 - \sqrt{(\mathrm{Corr} - 1)^2 + (\alpha - 1)^2 + (\beta - 1)^2} \tag{1}$$

$$\mathrm{NSE} = 1 - \frac{\sum_{t=1}^{N}(O_t - S_t)^2}{\sum_{t=1}^{N}(O_t - \mu_O)^2} \tag{2}$$

$$\mathrm{Corr} = \frac{\sum_{t=1}^{N}(O_t - \mu_O)(S_t - \mu_S)}{\sqrt{\sum_{t=1}^{N}(O_t - \mu_O)^2}\sqrt{\sum_{t=1}^{N}(S_t - \mu_S)^2}} \tag{3}$$

where O_t and S_t are the observed and simulated values at time t, over N time steps. The components of the KGE are the Pearson Correlation Coefficient (Corr), the variability ratio α (σ_S/σ_O), and the bias ratio β (μ_S/μ_O). μ_O and μ_S are the sample means, and σ_O and σ_S are the sample standard deviations of the observed and simulated series, respectively.

3 Results

3.1 Generalizability to unseen periods

In temporal generalization experiments, the regional model PLSTM-Reg outperforms the local model PLSTM-Loc across all three metrics in short-term prediction (Experiment I). At the 1-day lead time (Fig. 3 a–c), PLSTM-Reg achieves a median KGE of 0.96 versus 0.83 for PLSTM-Loc, and greatly reduces poorly simulated cases: reservoirs with KGE < 0.8 drop from 41.8% to 2.3%. PLSTM-Reg maintains its advantage across all lead times (1–7 days) (Fig. 3d) with statistically significant improvements (paired Wilcoxon signed-rank test, $p<0.05$). While the superior performance at the 1-day lead time may partly reflect the natural short-term persistence of reservoir systems, the model's ability to maintain high KGE at longer lead times suggests that it captures information relevant to reservoir operations beyond simple persistence. To further identify which reservoir types benefit the most, we stratified the performance (shown for the 1-day horizon) by primary operational purpose and regulation capacity (Fig. 3 e–f). PLSTM-Reg delivers significant improvements across all operational categories ($p<0.05$), with the largest gains for irrigation reservoirs. Improvements strongly correlate with regulation capacity: while local model accuracy drops sharply for reservoirs with large storage size ratios, the regional model remains consistently accurate, indicating that cross-reservoir learning helps capture the complex decision-making of heavily regulated systems. As for short-term storage prediction, both approaches achieve similarly high accuracy because storage is strongly constrained by the observed initial condition and exhibits substantial persistence over the 1–7 day prediction horizon (Supplementary Fig. S3). As daily inflows and releases are generally much smaller than total storage, differences in release prediction accuracy have limited influence on simulated storage over this short period.

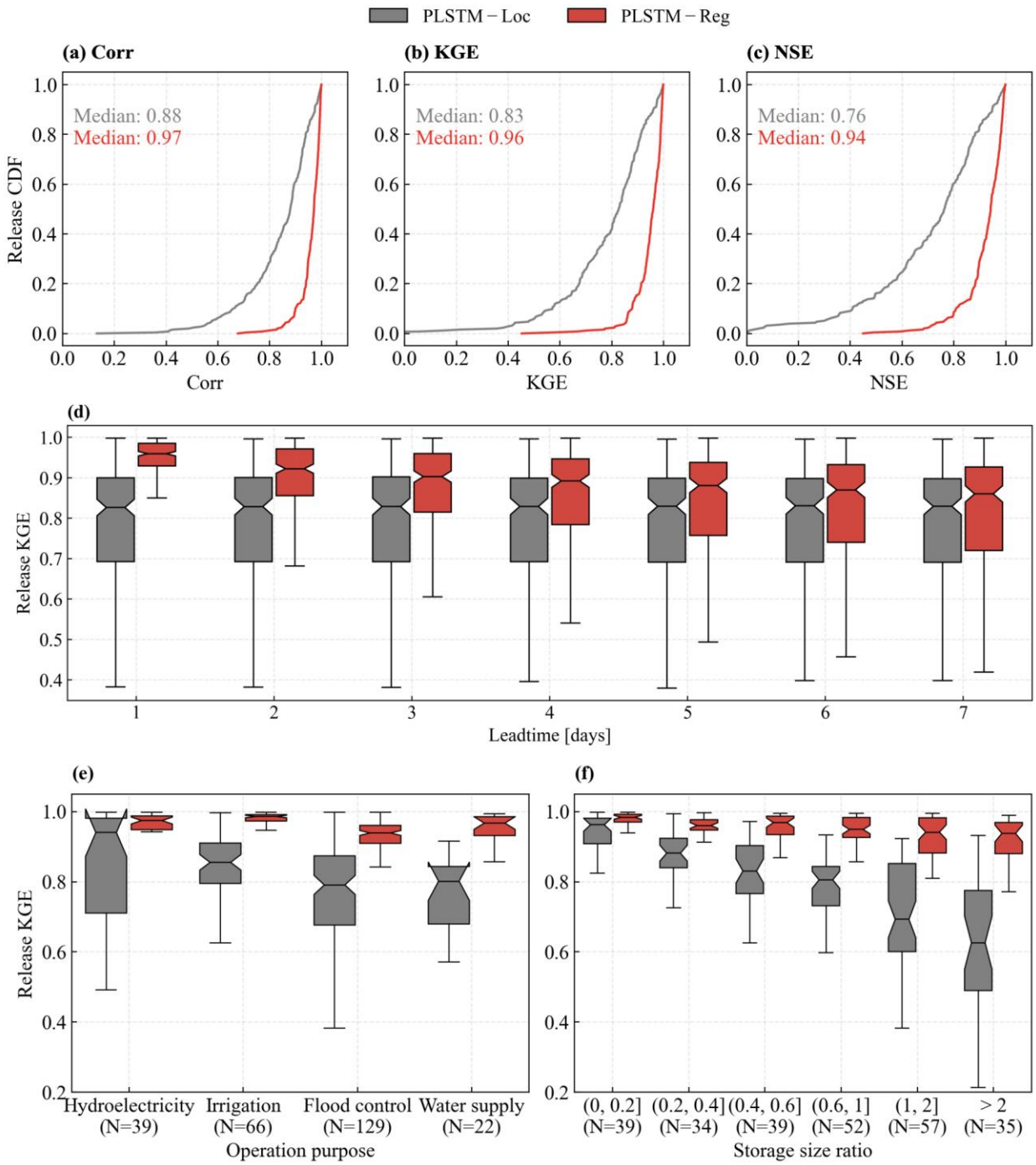


Figure 3. Evaluation of short-term release prediction performance (Experiment I) across all reservoirs during the test period. (a–c) Cumulative distribution functions (CDFs) of 1-day-ahead release metrics comparing regional and local models. Median scores are annotated. (d) Evolution of release KGE scores across lead times (1–7 days). (e–f) Performance stratified by (e) primary operational purpose and (f) storage size ratio. All paired comparisons shown in panels (d–f) are statistically significant based on the paired Wilcoxon signed-rank test ($p < 0.05$). N denotes the number of reservoirs in each category.

In long-term simulation (Experiment II), performance differences between the regional and local models are generally smaller than in short-term prediction (Experiment I). Overall, PLSTM-Reg offers only modest improvements in storage simulation (median storage KGE: 0.79 vs. 0.76; Supplementary Fig. S4), and release accuracy remains similar. Both PLSTM-Reg and PLSTM-Loc outperform the calibrated ISTARF benchmark, which achieves median KGE values of 0.64 for release and 0.47 for storage (Supplementary Fig. S4). Crucially, both models maintain long-term water balance with minimal systematic drift (median absolute release percent bias (|PBIAS|) below 0.4%; Supplementary Fig. S5). However, clear benefits emerge when examining specific reservoir groups. For reservoirs with storage size ratios > 0.2 (i.e., notable regulation capacity), the regional model performs notably better in the lower tail: the 25th percentile of storage KGE improves from 0.37 to 0.44, and the fraction of reservoirs with NSE < 0.5 declines from 34.1% to 29.0%. Together, these results suggest that while overall improvements narrow under long-term simulation, reflecting expected error accumulation, the regional model still provides meaningful robustness by mitigating failures in reservoir groups where the local model underperforms.

The robust performance gains, particularly for highly regulated systems, stem from a space-for-time substitution mechanism that allows the regional model to overcome the limitations of short local records. Complex multi-objective reservoirs (e.g., irrigation and flood control reservoirs) rely on rule structures triggered by specific hydroclimatic states that may never occur within a 15-year training record. For instance, a local model trained exclusively on wet periods cannot learn drought-hedging behavior. By pooling information from hundreds of reservoirs, the regional model absorbs operational strategies from "donor" sites and transfers them to those encountering similar, but locally unobserved conditions. This explains the substantial gains in systems with high regulation capacity (Fig. 3), where limited local data cannot represent the full range of decision-making complexity. Figure 4~~Figure 4~~ further illustrates this advantage using four reservoirs from geographically distinct regions that experience out-of-distribution events during the test period. Here, such events are defined as instances with test inflows, releases, or storage levels exceeding the training envelope by more than 20%. Local models struggle to extrapolate in such regimes, whereas the regional model consistently infers plausible release decisions. By learning generalized operating rules, the regional framework provides more reliable prediction and simulation, particularly as climate change increases the frequency of hydroclimatic extremes.

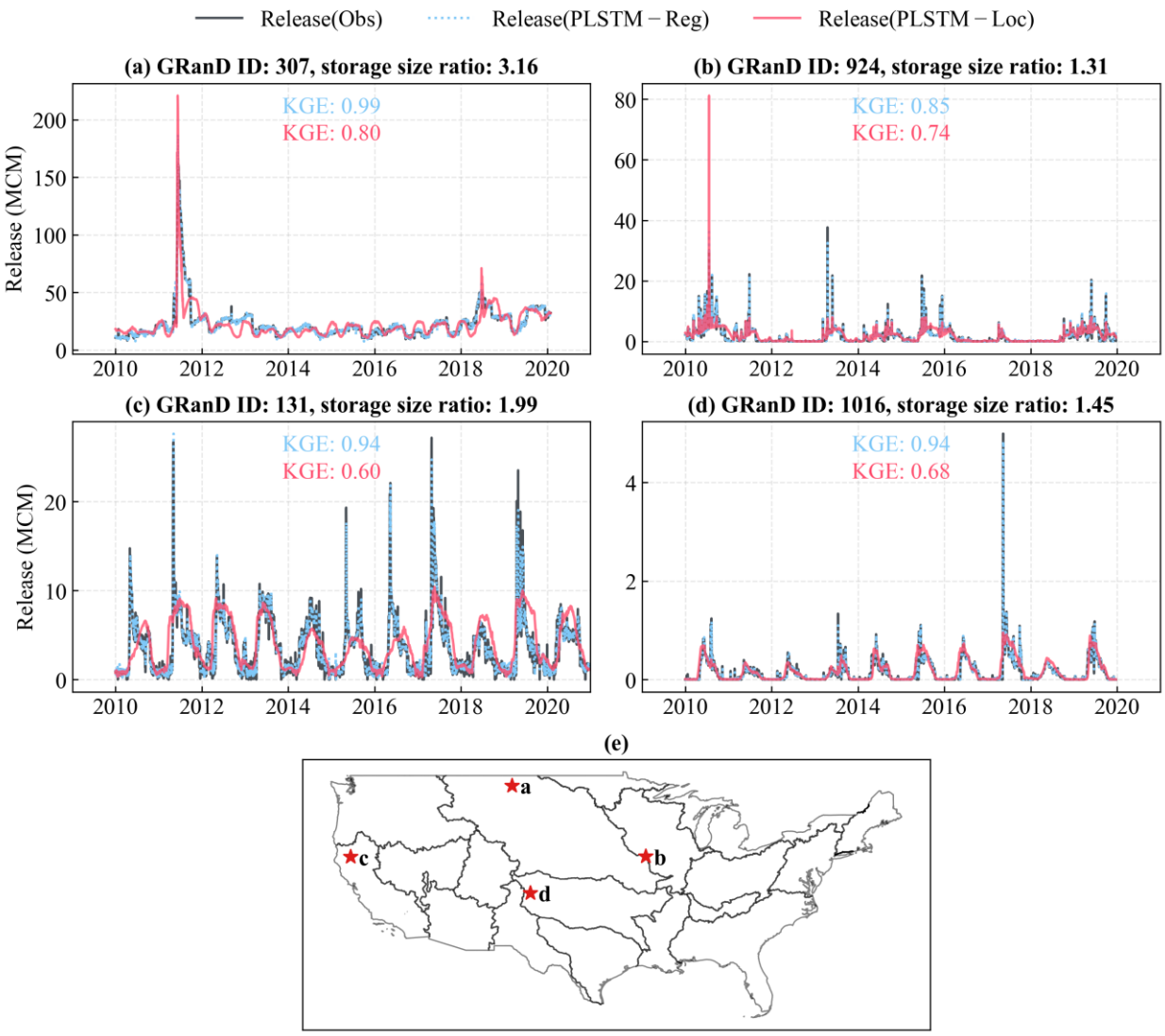


Figure 4. Release time series of four representative reservoirs illustrating the robustness of the regional model during out-of-distribution events at a 1-day lead time. (a)–(d) Release time series for four representative reservoirs; (e) The geographic locations of the selected reservoirs. Release values are expressed as daily total volume in million cubic meters (MCM).

Furthermore, we conducted a feature attribution analysis using the Integrated Gradients (Sundararajan et al., 2017) method (see Supplementary Text S3). The analysis shows that the model relies primarily on operational parameters (e.g., fill fraction, reservoir functions, and storage size ratio) together with regional topographic and hydroclimatic factors (e.g., elevation, precipitation, and temperature), whereas geometric variables (e.g., dam length, depth, and surface area) exert a comparatively minor influence (see Fig. S6).

3.2 Generalizability to unseen reservoirs

The regional framework demonstrates strong generalizability to unseen (data-scarce) reservoirs. In short-term prediction (Experiment III), PLSTM-Reg achieves a median 1-day-ahead KGE of 0.95 (Supplementary Fig. S7b) for reservoirs excluded from regional training. This performance exceeds that of the site-specific PLSTM-Loc models from Experiment I, which achieved a median KGE of 0.83 when trained using local historical records. The advantage of PLSTM-Reg persists across increasing lead times (Supplementary Fig. S7 g–h), indicating that the regional model can successfully transfer learned operating behaviors to previously unseen reservoirs. This generalization strength also holds in long-term simulation (Experiment IV). PLSTM-Reg markedly outperforms all rule-based benchmarks (Fig. 5), raising median release and storage KGE from 0.55 (ZAJC, best benchmark) to 0.73 and from 0.22 to 0.59, respectively. More importantly, the proportion of usable simulations improves sharply: reservoirs with release KGE > 0.5 increase from 56.6% (ZAJC) to 89.8%, and for storage from 14.4% to 61.7%. These results highlight the advantages of the proposed framework. The outperformance over generic and uncalibrated rule-based schemes reflects the combined effects of the nonlinear PLSTM architecture, regional data pooling, static reservoir attributes, and embedded physical constraints. Together, these components enable more realistic predictions in data-scarce settings where simplified empirical rules often fail.

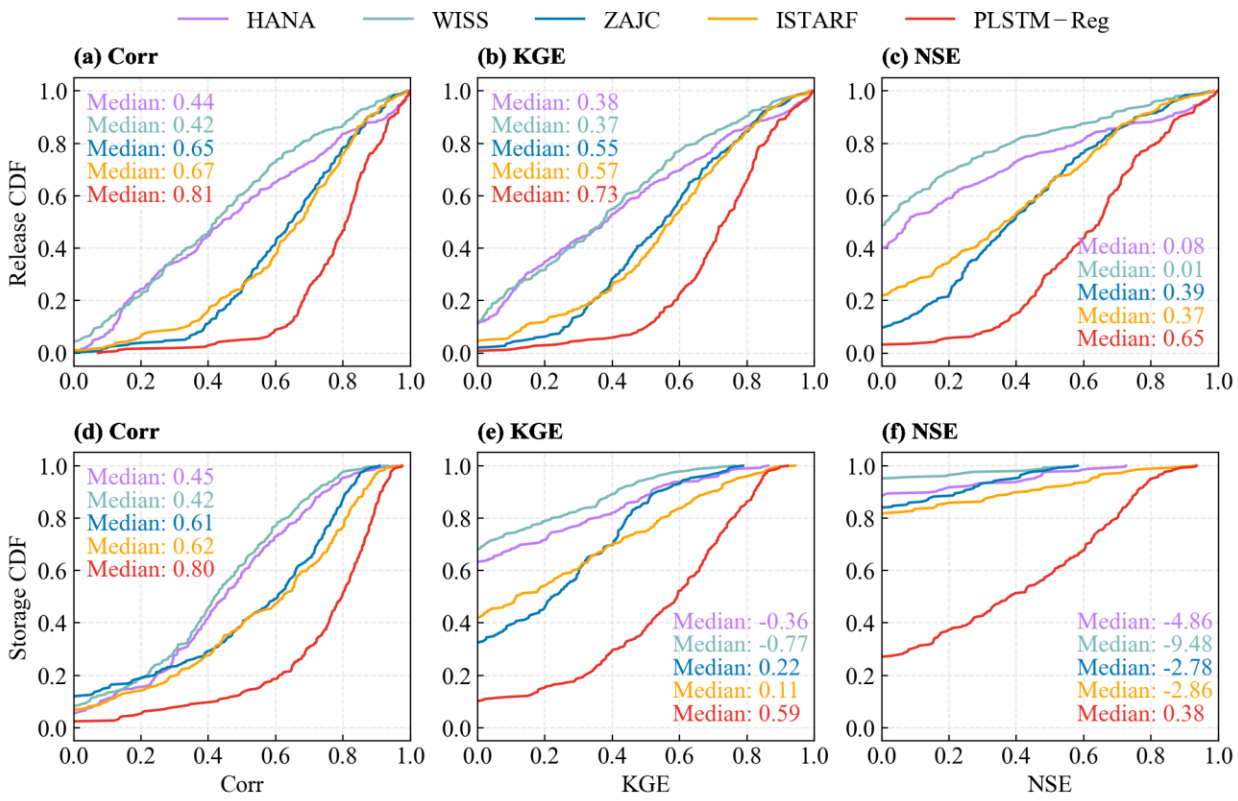


Figure 5. Comparison of release and storage long-term simulation performance (Experiment IV) between the regional model and four benchmark models. CDFs of three metrics (Corr, KGE, and NSE) are displayed for 256 reservoirs over the full evaluation period. The upper row (a–c) illustrates release performance, and the lower row (d–f) shows storage performance. Median metric values for each model are annotated within the respective panels.

In long-term simulation, performance gains remain statistically significant across reservoir groups differentiated by operational purpose and storage size ratio (Fig. 6). The largest improvements occur for flood control systems, particularly those in the Mississippi Basin (Supplementary Fig. S8), where PLSTM-Reg outperforms ZAJC by a median KGE of 0.24 for release and 0.53 for storage. This reflects the model's superior ability to capture the complex, event-driven operating rules. As exemplified in Supplementary Fig. S9 a–b, PLSTM-Reg holds releases low and stable during inflow peaks and increases discharge only after the flood peak has passed, closely matching observed flood mitigation strategies. In contrast, ZAJC releases rise synchronously with inflows, diverging from real-world practices and potentially amplifying downstream flood risks. Significant gains also emerge for irrigation and water supply reservoirs (Fig. 6), where PLSTM-Reg reproduces the seasonal release timing and transition patterns

characteristic of the western U.S. (exemplified in Supplementary Fig. S9 c–d). Performance advantages are also consistent across all storage size ratios (Fig. 6 c–d). For release, median KGE improvements exceed 0.1 for all but the smallest reservoirs (storage size ratio < 0.2). Storage gains are even larger, with improvements of >0.2 across all size classes (Fig. 6d). This consistent superiority demonstrates that the regional framework remains robust across a wide range of regulation regimes.

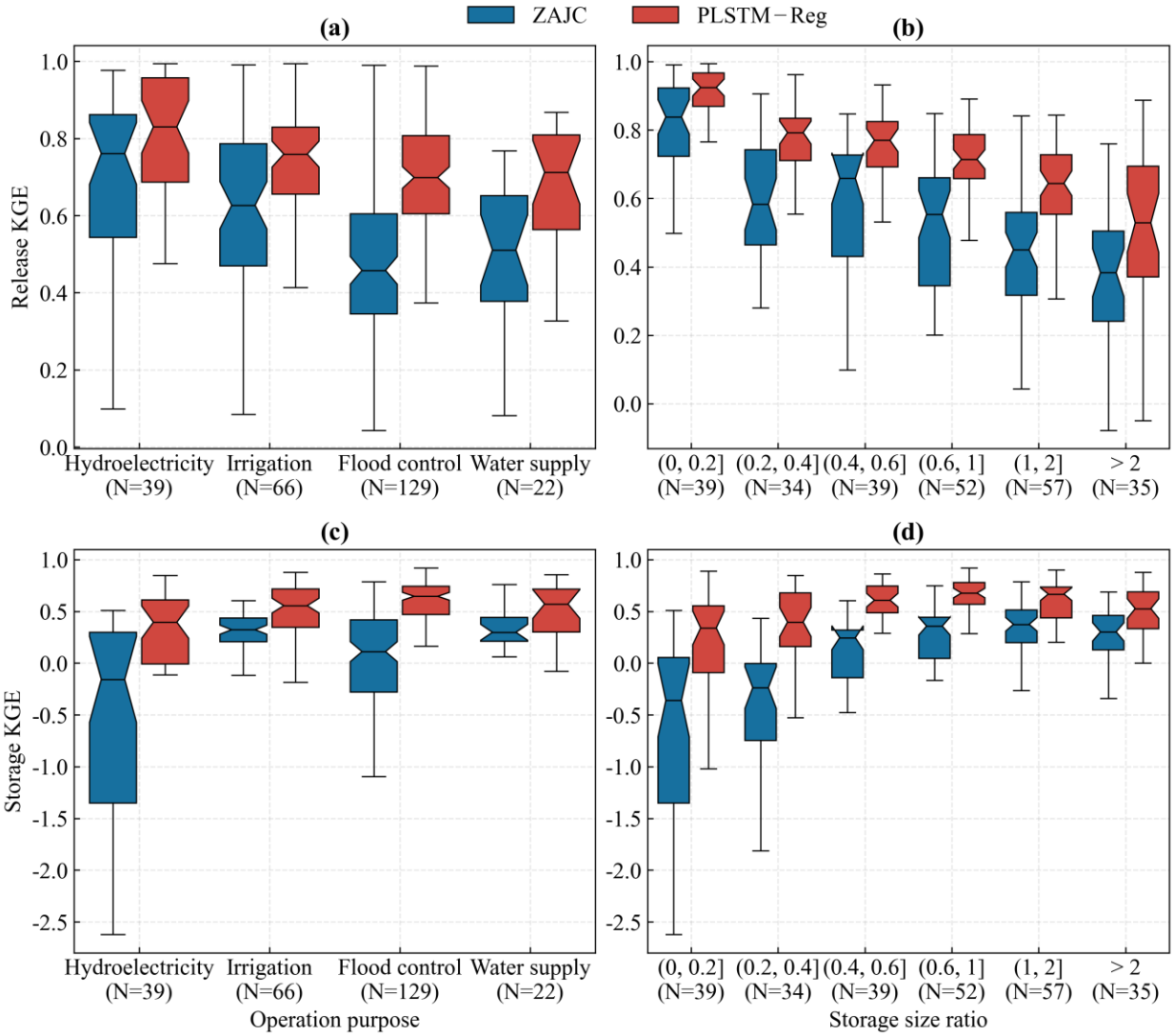
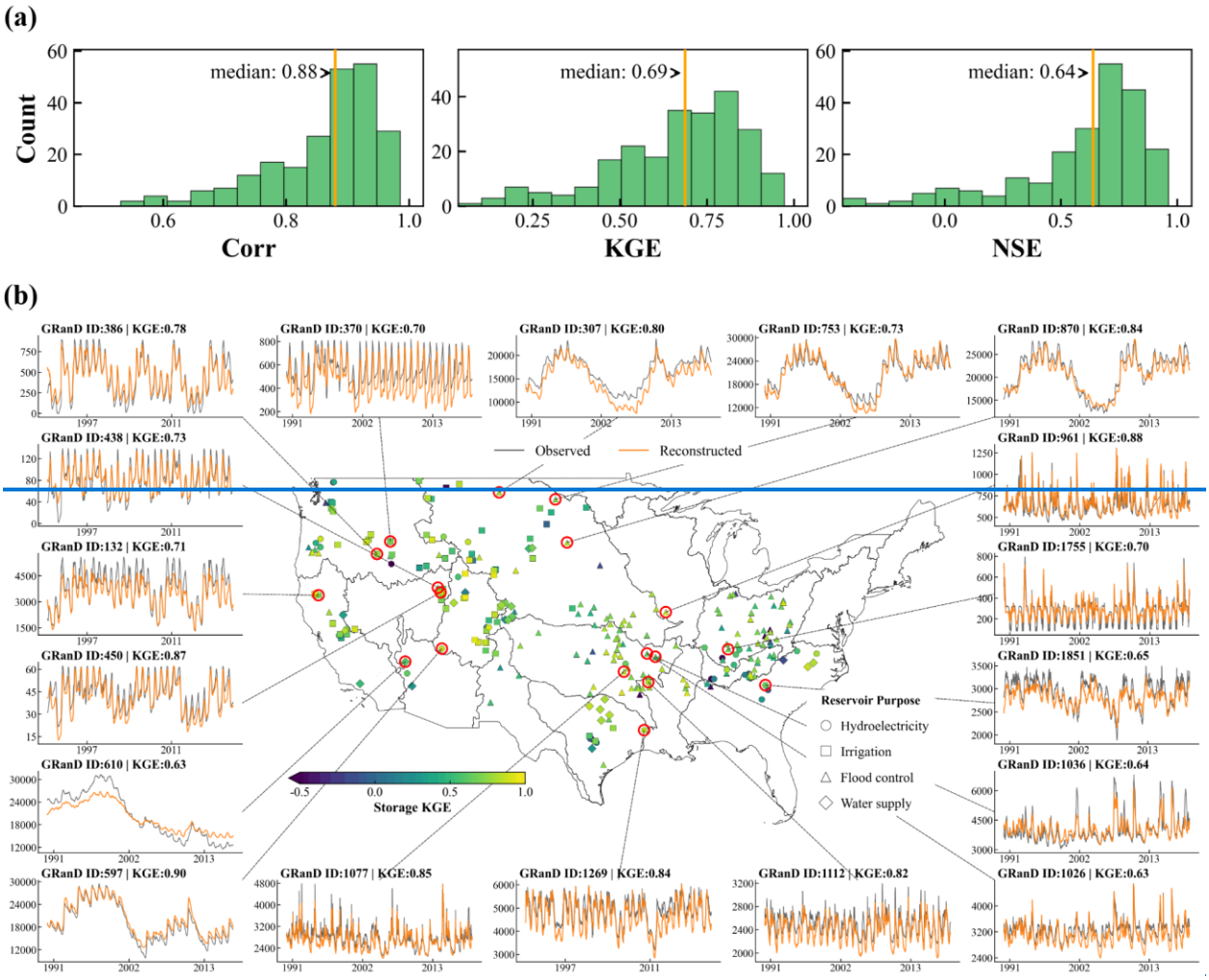


Figure 6. Long-term simulation performance comparison between the regional model (PLSTM-Reg) and the ZAJC benchmark for reservoir release (a, c) and storage (b, d), disaggregated by main operational purpose and storage size ratio. All paired comparisons are statistically significant based on the paired Wilcoxon signed-rank test ($p < 0.05$). N denotes the number of reservoirs in each category.

3.3 Reconstruction of historical records with remote-sensing support

Beyond the CONUS, site-specific reservoir operation records are scarce or inconsistently maintained worldwide. While PLSTM-Reg is able to partially fill this historical data gap through spatial generalization, as demonstrated in Sect. 3.2, its storage simulations remain far less accurate than releases (Fig. 5). Testing on the 256 U.S. reservoirs using cross-validation, Experiment V (PLSTM-Reg+RS) confirms that incorporating widely available monthly remote-sensing observations can guide the learning process and achieve robust storage performance, yielding a median KGE of 0.69 and an NSE of 0.64 (Fig. 7a). Notably, assimilating satellite data enables the regional model to outperform locally trained models (PLSTM-Loc, Experiment II): the proportion of reservoirs with acceptable storage performance (NSE > 0.5) increases to 64.5%, surpassing the 62.9% achieved by PLSTM-Loc (Supplementary Fig. S4). These results show that publicly available satellite data can effectively correct internal model states, serving as a substitute for missing ground-based records and enabling high-quality historical reconstruction in data-scarce reservoirs.

The spatial robustness of this reconstruction is visualized in Fig. 7b, which compares simulated and observed daily storage trajectories across 18 representative reservoirs spanning diverse hydroclimatic regimes. The model demonstrates high fidelity across a continuum of regulation dynamics, ranging from the humid, inflow-driven systems of the Ohio and Tennessee River basins (characterized by strong seasonal refill cycles) to the arid, storage-driven systems of the Colorado River basin. Crucially, the model captures multi-decadal trends in highly regulated systems, exemplified by the sustained depletion tracks of Lake Mead (GRanD ID 610) and Lake Powell (GRanD ID 597). This capability is particularly valuable for large irrigation and water supply reservoirs in the arid western U.S. These large systems typically operate under “storage-driven” hedging policies (Li et al., 2024), where release decisions depend on storage availability to ensure supply reliability during dry periods. In such regimes, the RS-based surface area series acts as a critical state correction by effectively mitigating the error accumulation in long-term simulation. Consequently, the median storage KGE exceeds 0.7 for all primary reservoir purposes (with the exception of small hydroelectric systems; Supplementary Fig. S10), confirming the framework as a robust strategy for reconstructing historical records across diverse data-scarce reservoirs.


(a)
Count
median: 0.88
Corr
median: 0.69
KGE
median: 0.64
NSE
(b)
GRanD ID:386 | KGE:0.78
GRanD ID:370 | KGE:0.70
GRanD ID:307 | KGE:0.80
GRanD ID:753 | KGE:0.73
GRanD ID:870 | KGE:0.84
GRanD ID:438 | KGE:0.73
Observed
Reconstructed
GRanD ID:961 | KGE:0.88
GRanD ID:132 | KGE:0.71
GRanD ID:1755 | KGE:0.70
GRanD ID:450 | KGE:0.87
GRanD ID:1851 | KGE:0.65
Reservoir Purpose
Hydroelectricity
Irrigation
Flood control
Water supply
GRanD ID:610 | KGE:0.63
Storage KGE
GRanD ID:1036 | KGE:0.64
GRanD ID:597 | KGE:0.90
GRanD ID:1077 | KGE:0.85
GRanD ID:1269 | KGE:0.84
GRanD ID:1112 | KGE:0.82
GRanD ID:1026 | KGE:0.63

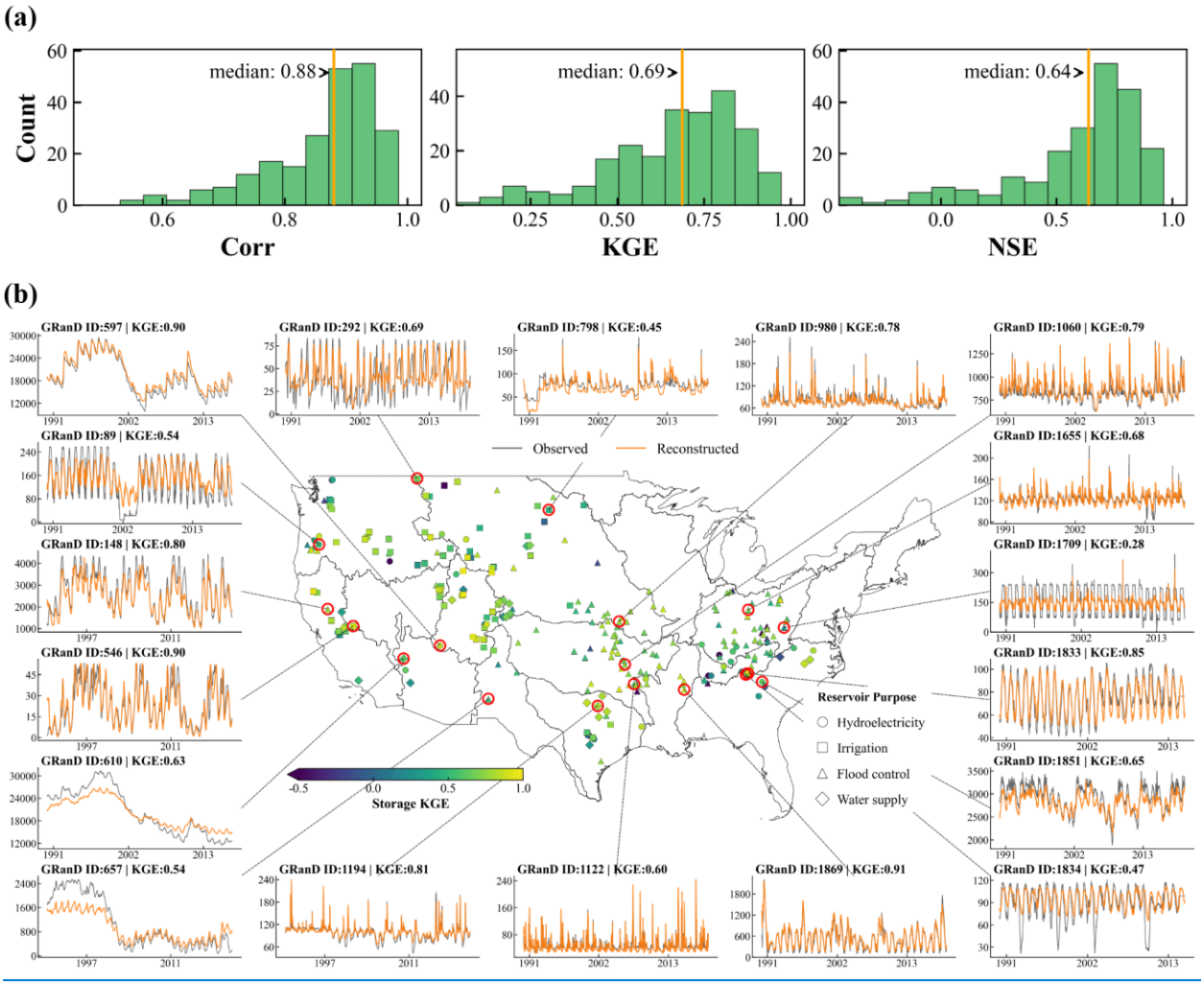


Figure 7. Evaluation of remote-sensing-augmented historical storage reconstruction (PLSTM-Reg+RS). (a) Overall reconstruction performance. Histograms show the distribution of Correlation, KGE, and NSE across the 256 U.S. reservoirs over the full data period. Orange vertical lines mark the median values. For visualization clarity, statistical outliers (values outside 1.5 × the interquartile range) are excluded. (b) Spatiotemporal analysis of the PLSTM-Reg+RS reconstruction. The central map illustrates the spatial distribution of KGE scores (color). Surrounding panels display storage time series for 18 ~~representative~~ reservoirs selected from reservoirs with storage size ratio > 0.2 using KGE-quartile-stratified random sampling ~~to~~ covering 1~~4~~5 HUC2 regions. Orange and gray lines represent model estimates and in situ measurements, respectively (units: million cubic meters).

4 Discussion

4.1 Short-term prediction vs. long-term simulation

The proposed physics-encoded regional framework demonstrates strong temporal generalizability to unseen periods, while its performance differs between short-term prediction and long-term simulation tasks. In short-term prediction, the model is continuously updated with recent storage observations, which implicitly correct prediction trajectories. Conversely, long-term simulation is performed without corrective feedback from observations, making the model highly susceptible to error accumulation. To investigate how these task-specific characteristics influence model behavior, we examine the role of static reservoir attributes by comparing the standard PLSTM-Reg model against a variant without static attributes (PLSTM-Reg-NA). For short-term prediction (1–7 days), removing static attributes has negligible impact (Supplementary Fig. S11), suggesting that predictions are primarily driven by dynamic inputs. In contrast, long-term simulation performance degrades substantially without static attributes (Fig. 8), with the median storage NSE decreasing from 0.69 to 0.21. The impact is most pronounced for reservoirs with storage size ratio > 0.2, where the proportion of simulation failures (NSE < 0) increases from 9.2% in the standard model to 42.4% in the NA variant.

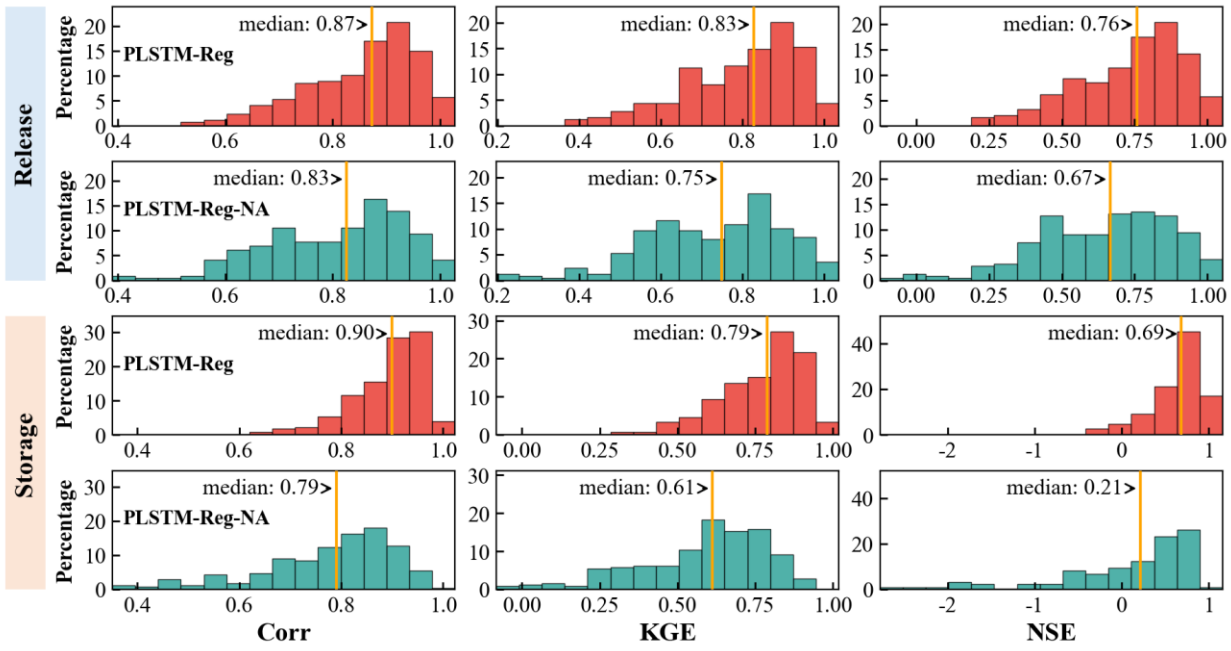


Figure 8. Comparison of long-term simulation performance between the standard regional model (PLSTM-Reg) and the variant without static attributes (PLSTM-Reg-NA). Histograms show the distribution of Correlation, KGE, and NSE for Release (top two rows)

and Storage (bottom two rows) during the test period. Orange vertical lines mark the median values. For visualization clarity, statistical outliers (values outside 1.5 × the interquartile range) are excluded.

These results underscore the distinct demands of the two tasks. In short-term prediction, storage observations provide strong reservoir state information, and the model aims to learn general, state-dependent rules, making site-specific attributes redundant. For example, a storage value near maximum capacity typically requires a high release decision to avoid overtopping, regardless of the reservoir purpose and size. In contrast, long-term simulation lacks corrective state feedback. In this setting, static attributes act as essential "anchors" that define the reservoir's operational identity, enabling the model to adhere to appropriate operational policies for each site and prevent long-term deviation. Specifically, static attributes enable the model to distinguish between different operation strategies, such as multi-year drought management in the arid Upper Colorado region versus seasonal flood control in the humid Ohio region.

4.2 Applications of the framework ~~and future directions~~

Our physics-encoded regional framework has broad potential applications in both real-time water management and long-term water planning. Accurate short-term release forecasts are increasingly important as climate change intensifies hydrological extremes (Gudmundsson et al., 2021; Iles et al., 2024). By capturing realistic decision rules from data, the model can serve as an effective tool for real-time decision support, aiding the assessment of flood and drought risks in complex reservoir systems (García-Feal et al., 2022; Yang et al., 2019). In addition, the regional model has a strong spatial generalization ability (Supplementary Fig. S7) to previously unseen reservoirs ~~with limited or no historical observations~~, offering a transferable baseline for reservoir operation prediction without site-specific model training~~reliable baseline forecast for newly commissioned or data-scarce systems~~ and thereby supporting applications in data-scarce systems.

For long-term simulation, the framework offers a physically constrained, operationally realistic alternative to the static, rule-based modules currently used in Global Hydrological Models (GHMs) and Earth System Models (ESMs). This is particularly valuable for future climate change resilience assessments, allowing policymakers to evaluate system vulnerabilities under altered inflow patterns (Longyang and Zeng, 2024). Furthermore, the integration of remote sensing (PLSTM-Reg+RS, Experiment V) is promising for historical data reconstruction. Unlike

traditional reconstruction methods constrained by satellite orbital tracks and cloud contamination (Dong et al., 2023b; Wu et al., 2022), our approach delivers continuous, daily-scale records. This is critical for closing the terrestrial water storage (TWS) budget, where anthropogenic reservoir storage change remains a major but poorly constrained component (An et al., 2026; Cooley et al., 2021; Dong et al., 2022). The reconstructed dataset can be further integrated into existing modeling workflows to improve representations of the human-modified water cycle.

It is worth noting that the framework is not tied to the net inflow used in this study as a required forcing. Rather, depending on data availability and the configuration of the host hydrological model, it can be driven by either observed or simulated reservoir inflow, or by net inflow that incorporates other reservoir gains and losses (Yu et al., 2025). In the present large-sample experiments, we used the net inflow provided by Chen et al. (2025) because consistent long-term inflow records are unavailable across the evaluated reservoirs. Although this dataset-provided net inflow was derived from reservoir observations to close the water balance, it does not mathematically constrain simulated storage to follow observations; storage errors still accumulate from release errors (see Supplementary Text S4 for details). Accordingly, the spatial-generalization experiments evaluate the transferability of learned reservoir operation behavior under prescribed hydrological forcing, whereas in large-scale hydrological applications the required forcing can be supplied directly by the host model.

4.3 Future directions

A critical next step is expanding the regional framework from continental to global scales. While our results demonstrate the efficacy of regional learning in the U.S., achieving a truly universal model requires compiling global datasets of historical operations. Expanding training diversity is a proven path to performance gains in deep learning hydrology (Kratzert et al., 2024). To handle global heterogeneity in operating rules, future work should explore domain adaptation techniques to improve model transferability across diverse policy paradigms (Shi and Cai, 2025). Alongside geographical expansion, future development may also extend the framework to cascading reservoir systems. The current PLSTM-Reg framework is designed for single-reservoir simulation, with upstream operational effects represented implicitly through downstream inflows. Extension to multi-reservoir systems could be achieved by coupling PLSTM-Reg with a river routing module that routes upstream releases to downstream reservoirs.

In addition, emerging technologies offer opportunities to refine model inputs and architecture. High-resolution elevation data from the Surface Water and Ocean Topography (SWOT) mission (Das and Hossain, 2025) can serve as a critical data assimilation source to correct simulation trajectories in data-scarce reservoirs. Furthermore, the model's static embeddings could be enhanced by geospatial foundation models (e.g., Google's AlphaEarth Foundations; Brown et al., 2025). Finally, integrating Generative AI offers a powerful avenue for enhancing short-term operational robustness. By using probabilistic inflow ensembles from diffusion-based forecasting models (Ou et al., 2025; Yang et al., 2025), the PLSTM-Reg v1.0 framework could be adapted to quantify operational uncertainty, enabling operators to move beyond deterministic predictions and make robust, risk-aware release decisions during extreme events.

5 Conclusions

This study shows that reservoir operations can be simulated robustly using PLSTM-Reg v1.0, a regional physics-encoded deep learning model trained across many reservoirs with high-quality data. Three key insights emerge. First, regional learning delivers clear gains in temporal generalization. Short-term release predictions improve substantially over local models, and low-skill cases are largely eliminated, particularly for reservoirs with high storage capacity or multiple objectives that require diverse operating responses. These benefits demonstrate that information learned from other reservoirs can compensate for limited training data of individual reservoirs. Second, strong spatial transfer confirms that reservoir operation rules contain learnable structure that can be generalized. When applied to unseen reservoirs, the model consistently outperforms widely used rule-based schemes for both release and storage, and the fraction of usable simulations increases across operational purposes and regulation strengths. This result indicates that the combination of a physics-encoded neural network architecture, regional training, and static reservoir attributes can capture shared behavioral patterns more effectively than simplified empirical rules, providing a more reliable basis for simulating reservoirs with limited or no operational records. Third, incorporating satellite-derived surface area enables credible reconstruction of storage dynamics in data-scarce settings, producing accuracy comparable to models trained on complete observations. This demonstrates the practical value of integrating

remote sensing into regional learning frameworks and highlights opportunities to fill historical gaps in poorly monitored systems.

Together, these findings establish that cross-reservoir deep learning, guided by physical constraints and supported by remote sensing, provides a scalable pathway for simulating human water management at regional and continental scales. The PLSTM-Reg framework offers immediate benefits as a transferable reservoir module in large-scale hydrological modeling and helps to quantify anthropogenic water storage change—particularly as global water systems evolve under climate change. Future work should focus on applying this framework globally, coupling it with existing hydrological and land surface models, and integrating emerging technologies such as geospatial foundation models and generative AI to further improve transferability, robustness, and operational utility.

Appendix A

Table A1. List of the 21 static reservoir attributes used in this study, including reservoir physical characteristics, operational purpose, and watershed climate descriptors.

Name	Unit	Description
Dam height	meters	Height of dam
Dam length	meters	Length of dam
Area	square kilometers	Representative surface area of reservoir
Capacity	million cubic meters	Representative maximum storage capacity of reservoir
Depth	meters	Average depth of reservoir, calculated as ratio between storage capacity and surface area
Elevation	meters	Elevation of reservoir surface above sea level
Catchment area	square kilometers	Area of upstream catchment draining into the reservoir
Mean discharge	liters per second	Long-term mean discharge at dam location
Storage size ratio	/	Ratio between storage capacity and total annual flow
Fill fraction	/	Long-term mean fraction of reservoir capacity filled
USE_IRRI	/	Used for irrigation (1: ‘Main’, 0: ‘Sec’, -1: ‘None’)
USE_ELEC	/	Used for hydroelectricity production (1: ‘Main’, 0: ‘Sec’, -1: ‘None’)

USE_SUPP	/	Used for water supply (1: 'Main', 0: 'Sec', -1: 'None')
USE_FCON	/	Used for flood control (1: 'Main', 0: 'Sec', -1: 'None')
USE_RECR	/	Used for recreation (1: 'Main', 0: 'Sec', -1: 'None')
USE_NAVI	/	Used for navigation (1: 'Main', 0: 'Sec', -1: 'None')
USE_FISH	/	Used for fisheries (1: 'Main', 0: 'Sec', -1: 'None')
USE_OTHR	/	Used for other purposes (1: 'Main', 0: 'Sec', -1: 'None')
Mean temperature	degrees Celsius	Long-term mean temperature
Mean precipitation	millimeters	Long-term mean precipitation
Aridity index	/	Index of climate dryness, ratio of potential evapotranspiration to precipitation

Notes: 'Main' refers to the primary purpose; 'Sec' refers to a secondary purpose; 'None' refers to no purpose.

Code and data availability

The reservoir operation dataset (Chen et al., 2025) and the processed meteorological forcings derived from Daymet (Thornton et al., 2022) used in this study have been permanently archived on Zenodo at **https://doi.org/10.5281/zenodo.19334272** (Yu et al., 2026b). Static reservoir attributes were obtained from the Global Dam Watch (GDW) database, available via Figshare at **https://doi.org/10.6084/m9.figshare.25988293** (Lehner et al., 2024). The Global Aridity Index dataset is available from Figshare at **https://doi.org/10.6084/m9.figshare.7504448** (Zomer et al., 2022). Catchment delineation relied on MERIT-Hydro raster data (Yamazaki et al., 2019), and MERIT-Basins vector data (Lin et al., 2019). The time-series surface area dynamics for the evaluated reservoirs were provided by the Global Reservoir Surface Area Dataset (GRSAD; Zhao and Gao, 2018). To ensure reproducibility and compliance with long-term archiving requirements, the specific subsets of raster, vector, and surface area data used for the evaluated reservoirs have been bundled and permanently archived on Zenodo at **https://doi.org/10.5281/zenodo.19284811** (Yu et al., 2026a).

Catchment delineation was performed using the delineator package, available at **https://doi.org/10.5281/zenodo.7314286** (Heberger, 2023). The model training and evaluation framework was built using the open-source NeuralHydrology Python library, available at

https://doi.org/10.5281/zenodo.7063258 (Kratzert et al., 2022). The PLSTM-Reg v1.0 model used in this study is archived at **https://doi.org/10.5281/zenodo.18265198** (Yu, 2026).

Supplement

The supplement related to this article is available.

Author contributions

BY and YZ conceptualized the study. All authors contributed to the methodology and formal analysis. BY and YC were responsible for data curation and visualization. BY performed the validation and prepared the original draft. YC and YZ reviewed and edited the manuscript. YZ was responsible for supervision, project administration, and funding acquisition.

Competing interests

The contact author has declared that none of the authors has any competing interests.

Disclaimer

Publisher's note: Copernicus Publications remains neutral with regard to jurisdictional claims made in the text, published maps, institutional affiliations, or any other geographical representation in this paper. While Copernicus Publications makes every effort to include appropriate place names, the final responsibility lies with the authors.

Acknowledgements

We acknowledge the availability of high-resolution satellite imagery from Google Earth, which was essential for the manual verification and correction of dam locations during catchment delineation. The computational resources used in this study were supported by the Center for Computational Science and Engineering at Southern University of Science and Technology. AI tools were used to improve the grammar and fluency of the manuscript.

Financial support

This research has been supported by the National Natural Science Foundation of China (grant nos. 42325702 and 42407072).

References

An, Z., Li, Z., Jin, T., Jiang, W., Yuan, P., Liu, K., Wang, J., and Chen, P.: Water Storage Changes of Lakes and Reservoirs Across Asia (2018–2023) and Their Effects in Flood Control, Geophys. Res. Lett., 53, e2025GL119131, https://doi.org/10.1029/2025GL119131, 2026.

Brown, C. F., Kazmierski, M. R., Pasquarella, V. J., Rucklidge, W. J., Samsikova, M., Zhang, C., Shelhamer, E., Lahera, E., Wiles, O., Ilyushchenko, S., Gorelick, N., Zhang, L. L., Alj, S., Schechter, E., Askay, S., Guinan, O., Moore, R., Boukouvalas, A., and Kohli, P.: AlphaEarth Foundations: An embedding field model for accurate and efficient global mapping from sparse label data, https://doi.org/10.48550/arXiv.2507.22291, 8 September 2025.

Chalise, D. R., Sankarasubramanian, A., and Ruhi, A.: Dams and Climate Interact to Alter River Flow Regimes Across the United States, Earths Future, 9, e2020EF001816, https://doi.org/10.1029/2020EF001816, 2021.

Chen, Y., Li, D., Zhao, Q., and Cai, X.: Developing a generic data-driven reservoir operation model, Adv. Water Resour., 167, 104274, https://doi.org/10.1016/j.advwatres.2022.104274, 2022.

Chen, Y., Cai, X., and Li, D.: Historical Operation Data of 256 Reservoirs in Contiguous United States, https://doi.org/10.4211/hs.092720588e2e4524bf2674235ff69d81, 2025.

Cheng, H., Wang, T., and Yang, D.: Quantifying the Regulation Capacity of the Three Gorges Reservoir on Extreme Hydrological Events and Its Impact on Flow Regime in a Changing Climate, Water Resour. Res., 60, e2023WR036329, https://doi.org/10.1029/2023WR036329, 2024.

Cooley, S. W., Ryan, J. C., and Smith, L. C.: Human alteration of global surface water storage variability, Nature, 591, 78–81, https://doi.org/10.1038/s41586-021-03262-3, 2021.

Cosgrove, B., Gochis, D., Flowers, T., Dugger, A., Ogden, F., Graziano, T., Clark, E., Cabell, R., Casiday, N., Cui, Z., Eicher, K., Fall, G., Feng, X., Fitzgerald, K., Frazier, N., George, C., Gibbs, R., Hernandez, L., Johnson, D., Jones, R., Karsten, L., Kefelegn, H., Kitzmiller, D., Lee, H., Liu, Y., Mashriqui, H., Mattern, D., McCluskey, A., McCreight, J. L., McDaniel, R., Midekisa, A., Newman, A., Pan, L., Pham, C., RafieeiNasab, A., Rasmussen, R., Read, L., Rezaeianzadeh, M., Salas, F., Sang, D., Sampson, K., Schneider, T., Shi, Q., Sood, G., Wood, A., Wu, W., Yates, D., Yu, W., and Zhang, Y.: NOAA's National Water Model: Advancing operational hydrology through continental-scale modeling, JAWRA J. Am. Water Resour. Assoc., 60, 247–272, https://doi.org/10.1111/1752-1688.13184, 2024.

Das, P. and Hossain, F.: Multi-Satellite Tracking of Surface Water Storage Change in the Era of Surface Water and Ocean Topography (SWOT) Satellite Mission, Earth Space Sci., 12, e2024EA004178, https://doi.org/10.1029/2024EA004178, 2025.

DeNeale, S. T., Baecher, G. B., Stewart, K. M., Smith, E. D., and Watson, D. B.: Current State-of-Practice in Dam Safety Risk Assessment, Oak Ridge National Laboratory (ORNL), Oak Ridge, TN (United States), https://doi.org/10.2172/1592163, 2019.

Dong, N., Wei, J., Yang, M., Yan, D., Yang, C., Gao, H., Arnault, J., Laux, P., Zhang, X., Liu, Y., Niu, J., Wang, H., Wang, H., Kunstmann, H., and Yu, Z.: Model Estimates of China's Terrestrial Water Storage Variation Due To Reservoir Operation, Water Resour. Res., 58, e2021WR031787, https://doi.org/10.1029/2021WR031787, 2022.

Dong, N., Guan, W., Cao, J., Zou, Y., Yang, M., Wei, J., Chen, L., and Wang, H.: A hybrid hydrologic modelling framework with data-driven and conceptual reservoir operation schemes for reservoir impact assessment and predictions, J. Hydrol., 619, 129246, https://doi.org/10.1016/j.jhydrol.2023.129246, 2023a.

Dong, N., Yang, M., Wei, J., Arnault, J., Laux, P., Xu, S., Wang, H., Yu, Z., and Kunstmann, H.: Toward Improved Parameterizations of Reservoir Operation in Ungauged Basins: A Synergistic Framework Coupling Satellite Remote Sensing, Hydrologic Modeling, and Conceptual Operation Schemes, Water Resour. Res., 59, e2022WR033026, https://doi.org/10.1029/2022WR033026, 2023b.

Fan, C., Song, C., Wang, J., Sheng, Y., Lin, Y., Yuan, C., Safat Sikder, M., Crétaux, J.-F., Liu, K., Chen, T., Zeng, F., and Ke, L.: Emerging global reservoirs in the new millennium: Abundance, hotspots, and total water storage, Sci. Bull., 69, 2179–2182, https://doi.org/10.1016/j.scib.2024.04.043, 2024.

Fang, K., Kifer, D., Lawson, K., Feng, D., and Shen, C.: The Data Synergy Effects of Time-Series Deep Learning Models in Hydrology, Water Resour. Res., 58, e2021WR029583, https://doi.org/10.1029/2021WR029583, 2022.

Ford, L. and Sankarasubramanian, A.: Generalizing Reservoir Operations Using a Piecewise Classification and Regression Approach, Water Resour. Res., 59, e2023WR034890, https://doi.org/10.1029/2023WR034890, 2023.

García-Feal, O., González-Cao, J., Fernández-Nóvoa, D., Astray Dopazo, G., and Gómez-Gesteira, M.: Comparison of machine learning techniques for reservoir outflow forecasting, Nat. Hazards Earth Syst. Sci., 22, 3859–3874, https://doi.org/10.5194/nhess-22-3859-2022, 2022.

Grill, G., Lehner, B., Thieme, M., Geenen, B., Tickner, D., Antonelli, F., Babu, S., Borrelli, P., Cheng, L., Crochetiere, H., Ehalt Macedo, H., Filgueiras, R., Goichot, M., Higgins, J., Hogan, Z., Lip, B., McClain, M. E., Meng, J., Mulligan, M., Nilsson, C., Olden, J. D., Opperman, J. J., Petry, P., Reidy Liermann, C., Sáenz, L., Salinas-Rodríguez, S., Schelle, P., Schmitt, R. J. P., Snider, J., Tan, F., Tockner, K., Valdujo, P. H., van Soesbergen, A., and Zarfl, C.: Mapping the world's free-flowing rivers, Nature, 569, 215–221, https://doi.org/10.1038/s41586-019-1111-9, 2019.

Gudmundsson, L., Boulange, J., Do, H. X., Gosling, S. N., Grillakis, M. G., Koutroulis, A. G., Leonard, M., Liu, J., Müller Schmied, H., Papadimitriou, L., Pokhrel, Y., Seneviratne, S.

I., Satoh, Y., Thiery, W., Westra, S., Zhang, X., and Zhao, F.: Globally observed trends in mean and extreme river flow attributed to climate change, Science, 371, 1159–1162, https://doi.org/10.1126/science.aba3996, 2021.

Gupta, H. V., Kling, H., Yilmaz, K. K., and Martinez, G. F.: Decomposition of the mean squared error and NSE performance criteria: Implications for improving hydrological modelling, J. Hydrol., 377, 80–91, https://doi.org/10.1016/j.jhydrol.2009.08.003, 2009.

Haemmerli, H. L., Gerlak, A. K., and Swanson, T.: Reimagining hydropower in the United States, WIREs Water, 11, e1735, https://doi.org/10.1002/wat2.1735, 2024.

Hanasaki, N., Kanae, S., Oki, T., Masuda, K., Motoya, K., Shirakawa, N., Shen, Y., and Tanaka, K.: An integrated model for the assessment of global water resources – Part 1: Model description and input meteorological forcing, Hydrol. Earth Syst. Sci., 12, 1007–1025, https://doi.org/10.5194/hess-12-1007-2008, 2008a.

Hanasaki, N., Kanae, S., Oki, T., Masuda, K., Motoya, K., Shirakawa, N., Shen, Y., and Tanaka, K.: An integrated model for the assessment of global water resources – Part 2: Applications and assessments, Hydrol. Earth Syst. Sci., 12, 1027–1037, https://doi.org/10.5194/hess-12-1027-2008, 2008b.

Heberger, M.: delineator.py: Fast, accurate watershed delineation using hybrid vector- and raster-based methods and data from MERIT-Hydro, , https://doi.org/10.5281/zenodo.7314286, 2023.

Iles, C. E., Samset, B. H., Sandstad, M., Schuhen, N., Wilcox, L. J., and Lund, M. T.: Strong regional trends in extreme weather over the next two decades under high- and low-emissions pathways, Nat. Geosci., 1–6, https://doi.org/10.1038/s41561-024-01511-4, 2024.

Kingma, D. P. and Ba, J.: Adam: A Method for Stochastic Optimization, in: ICLR (Poster), arXiv: 1412.6980, 2015.

Kratzert, F., Klotz, D., Herrnegger, M., Sampson, A. K., Hochreiter, S., and Nearing, G. S.: Toward Improved Predictions in Ungauged Basins: Exploiting the Power of Machine Learning, Water Resour. Res., 55, 11344–11354, https://doi.org/10.1029/2019WR026065, 2019.

Kratzert, F., Gauch, M., Nearing, G., and Klotz, D.: NeuralHydrology --- A Python library for Deep Learning research in hydrology, J. Open Source Softw., 7, 4050, https://doi.org/10.21105/joss.04050, 2022.

Kratzert, F., Gauch, M., Klotz, D., and Nearing, G.: HESS Opinions: Never train a Long Short-Term Memory (LSTM) network on a single basin, Hydrol. Earth Syst. Sci., 28, 4187–4201, https://doi.org/10.5194/hess-28-4187-2024, 2024.

Lehner, B., Liermann, C. R., Revenga, C., Vörösmarty, C., Fekete, B., Crouzet, P., Döll, P., Endejan, M., Frenken, K., Magome, J., Nilsson, C., Robertson, J. C., Rödel, R., Sindorf, N., and Wisser, D.: High-resolution mapping of the world's reservoirs and dams for sustainable river-flow management, Front. Ecol. Environ., 9, 494–502, https://doi.org/10.1890/100125, 2011.

Lehner, B., Beames, P., Mulligan, M., Zarfl, C., De Felice, L., van Soesbergen, A., Thieme, M., Garcia de Leaniz, C., Anand, M., Belletti, B., Brauman, K. A., Januchowski-Hartley, S. R.,

Lyon, K., Mandle, L., Mazany-Wright, N., Messager, M. L., Pavelsky, T., Pekel, J.-F., Wang, J., Wen, Q., Wishart, M., Xing, T., Yang, X., and Higgins, J.: The Global Dam Watch database of river barrier and reservoir information for large-scale applications, Sci. Data, 11, 1069, https://doi.org/10.1038/s41597-024-03752-9, 2024.

Li, D., Chen, Y., Lyu, L., and Cai, X.: Uncovering Historical Reservoir Operation Rules and Patterns: Insights From 452 Large Reservoirs in the Contiguous United States, Water Resour. Res., 60, e2023WR036686, https://doi.org/10.1029/2023WR036686, 2024.

Li, D., Vora, A., and Cai, X.: Streamflow simulation improvements enabled by a state-of-the-art algorithm for reservoir routing in the U.S. National Water Model, JAWRA J. Am. Water Resour. Assoc., 61, e13244, https://doi.org/10.1111/1752-1688.13244, 2025.

Lin, P., Pan, M., Beck, H. E., Yang, Y., Yamazaki, D., Frasson, R., David, C. H., Durand, M., Pavelsky, T. M., Allen, G. H., Gleason, C. J., and Wood, E. F.: Global Reconstruction of Naturalized River Flows at 2.94 Million Reaches, Water Resour. Res., 55, 6499–6516, https://doi.org/10.1029/2019WR025287, 2019.

Longyang, Q. and Zeng, R.: A Hierarchical Temporal Scale Framework for Data-Driven Reservoir Release Modeling, Water Resour. Res., 59, e2022WR033922, https://doi.org/10.1029/2022WR033922, 2023.

Longyang, Q. and Zeng, R.: Assessing the effectiveness of reservoir operation and identifying reallocation opportunities under climate change, Environ. Res. Lett., 19, 074010, https://doi.org/10.1088/1748-9326/ad5459, 2024.

mhpi: hydrodl2, GitHub [code], available at: https://github.com/mhpi/hydrodl2 (last access: 5 May 2026), 2026.

Nash, J. E. and Sutcliffe, J. V.: River flow forecasting through conceptual models part I — A discussion of principles, J. Hydrol., 10, 282–290, https://doi.org/10.1016/0022-1694(70)90255-6, 1970.

Ou, Z., Nai, C., Pan, B., Zheng, Y., Shen, C., Jiang, P., Liu, X., Tang, Q., Li, W., and Pan, M.: Probabilistic Diffusion Models Advance Extreme Flood Forecasting, Geophys. Res. Lett., 52, e2025GL115705, https://doi.org/10.1029/2025GL115705, 2025.

Paszke, A., Gross, S., Massa, F., Lerer, A., Bradbury, J., Chanan, G., Killeen, T., Lin, Z., Gimelshein, N., Antiga, L., Desmaison, A., Kopf, A., Yang, E., DeVito, Z., Raison, M., Tejani, A., Chilamkurthy, S., Steiner, B., Fang, L., Bai, J., and Chintala, S.: PyTorch: An Imperative Style, High-Performance Deep Learning Library, in: Advances in Neural Information Processing Systems, 2019.

Shen, Y., Yamazaki, D., Pokhrel, Y., and Zhao, G.: Improving Global Reservoir Parameterizations by Incorporating Flood Storage Capacity Data and Satellite Observations, Water Resour. Res., 61, e2024WR037620, https://doi.org/10.1029/2024WR037620, 2025.

Shi, H. and Cai, X.: Extrapolability improvement of machine learning-based evapotranspiration models via domain-adversarial neural networks, Environ. Model. Softw., 187, 106383, https://doi.org/10.1016/j.envsoft.2025.106383, 2025.

Steyaert, J. C. and Condon, L. E.: Synthesis of historical reservoir operations from 1980 to 2020 for the evaluation of reservoir representation in large-scale hydrologic models, Hydrol. Earth Syst. Sci., 28, 1071–1088, https://doi.org/10.5194/hess-28-1071-2024, 2024.

Steyaert, J. C., Sutanudjaja, E., Bierkens, M., and Wanders, N.: A data derived workflow for reservoir operations for simulating reservoir operations in a global hydrologic model, EGUsphere, 1–38, https://doi.org/10.5194/egusphere-2024-3658, 2025.

Sundararajan, M., Taly, A., and Yan, Q.: Axiomatic Attribution for Deep Networks, ArXiv170301365 Cs, 2017.

Sutanudjaja, E. H., van Beek, R., Wanders, N., Wada, Y., Bosmans, J. H. C., Drost, N., van der Ent, R. J., de Graaf, I. E. M., Hoch, J. M., de Jong, K., Karssenberg, D., López López, P., Peßenteiner, S., Schmitz, O., Straatsma, M. W., Vannametee, E., Wisser, D., and Bierkens, M. F. P.: PCR-GLOBWB 2: a 5 arcmin global hydrological and water resources model, Geosci. Model Dev., 11, 2429–2453, https://doi.org/10.5194/gmd-11-2429-2018, 2018.

Thornton, M. M., Shrestha, R., Wei, Y., Thornton, P. E., and Kao, S.-C.: Daymet: Daily Surface Weather Data on a 1-km Grid for North America (4.1), https://doi.org/10.3334/ORNLDAAC/2129, 2022.

Thornton, P. E., Shrestha, R., Thornton, M., Kao, S.-C., Wei, Y., and Wilson, B. E.: Gridded daily weather data for North America with comprehensive uncertainty quantification, Sci. Data, 8, 190, https://doi.org/10.1038/s41597-021-00973-0, 2021.

Tran, H., Zhou, T., Tan, Z., Fang, Y., and Ruby Leung, L.: Improving the prediction of daily reservoir releases over the CONUS using conditioned LSTM, J. Hydrol., 661, 133750, https://doi.org/10.1016/j.jhydrol.2025.133750, 2025.

Turner, S. W. D., Doering, K., and Voisin, N.: Data-Driven Reservoir Simulation in a Large-Scale Hydrological and Water Resource Model, Water Resour. Res., 56, e2020WR027902, https://doi.org/10.1029/2020WR027902, 2020.

Turner, S. W. D., Steyaert, J. C., Condon, L., and Voisin, N.: Water storage and release policies for all large reservoirs of conterminous United States, J. Hydrol., 603, 126843, https://doi.org/10.1016/j.jhydrol.2021.126843, 2021.

Vora, A., Cai, X., Chen, Y., and Li, D.: Coupling Reservoir Operation and Rainfall-Runoff Processes for Streamflow Simulation in Watersheds, Water Resour. Res., 60, e2023WR035703, https://doi.org/10.1029/2023WR035703, 2024.

Wisser, D., Fekete, B. M., Vörösmarty, C. J., and Schumann, A. H.: Reconstructing 20th century global hydrography: a contribution to the Global Terrestrial Network- Hydrology (GTN-H), Hydrol. Earth Syst. Sci., 14, 1–24, https://doi.org/10.5194/hess-14-1-2010, 2010.

Wu, G., Xiao, X., and Liu, Y.: Satellite-Based Surface Water Storage Estimation: Its history, current status, and future prospects, IEEE Geosci. Remote Sens. Mag., 10, 10–31, https://doi.org/10.1109/MGRS.2022.3175159, 2022.

Yamazaki, D., Ikeshima, D., Sosa, J., Bates, P. D., Allen, G. H., and Pavelsky, T. M.: MERIT Hydro: A High-Resolution Global Hydrography Map Based on Latest Topography Dataset, Water Resour. Res., 55, 5053–5073, https://doi.org/10.1029/2019WR024873, 2019.

Yang, S., Yang, D., Chen, J., and Zhao, B.: Real-time reservoir operation using recurrent neural networks and inflow forecast from a distributed hydrological model, J. Hydrol., 579, 124229, https://doi.org/10.1016/j.jhydrol.2019.124229, 2019.

Yang, T., Gao, X., Sorooshian, S., and Li, X.: Simulating California reservoir operation using the classification and regression-tree algorithm combined with a shuffled cross-validation scheme, Water Resour. Res., 52, 1626–1651, https://doi.org/10.1002/2015WR017394, 2016.

Yang, T., Zhang, L., Kim, T., Hong, Y., Zhang, D., and Peng, Q.: A large-scale comparison of Artificial Intelligence and Data Mining (AI&DM) techniques in simulating reservoir releases over the Upper Colorado Region, J. Hydrol., 602, 126723, https://doi.org/10.1016/j.jhydrol.2021.126723, 2021.

Yang, W., Ji, H., Lonzarich, L., Song, Y., and Shen, C.: Diffusion-Based Probabilistic Modeling for Hourly Streamflow Prediction and Assimilation, https://doi.org/10.48550/arXiv.2510.08488, 9 October 2025.

Yassin, F., Razavi, S., Elshamy, M., Davison, B., Sapriza-Azuri, G., and Wheater, H.: Representation and improved parameterization of reservoir operation in hydrological and land-surface models, Hydrol. Earth Syst. Sci., 23, 3735–3764, https://doi.org/10.5194/hess-23-3735-2019, 2019.

Yu, B.: PLSTM-Reg v1.0: A regional physics-encoded LSTM model for simulating reservoir operations under data scarcity, , https://doi.org/10.5281/zenodo.18265198, 2026.

Yu, B., Zheng, Y., He, S., Xiong, R., and Wang, C.: Physics-encoded deep learning for integrated modeling of watershed hydrology and reservoir operations, J. Hydrol., 657, 133052, https://doi.org/10.1016/j.jhydrol.2025.133052, 2025.

Yu, B., Chen, Y., and Zheng, Y.: MERIT and GRSAD Subsets (CONUS) for PLSTM-Reg v1.0 Reservoir Modeling, https://doi.org/10.5281/zenodo.19284811, 2026a.

Yu, B., Chen, Y., and Zheng, Y.: Meteorological Forcings and Reservoir Operations Data for PLSTM-Reg v1.0 (CONUS), https://doi.org/10.5281/zenodo.19334272, 2026b.

Zajac, Z., Revilla-Romero, B., Salamon, P., Burek, P., Hirpa, F. A., and Beck, H.: The impact of lake and reservoir parameterization on global streamflow simulation, J. Hydrol., 548, 552–568, https://doi.org/10.1016/j.jhydrol.2017.03.022, 2017.

Zhang, D., Lin, J., Peng, Q., Wang, D., Yang, T., Sorooshian, S., Liu, X., and Zhuang, J.: Modeling and simulating of reservoir operation using the artificial neural network, support vector regression, deep learning algorithm, J. Hydrol., 565, 720–736, https://doi.org/10.1016/j.jhydrol.2018.08.050, 2018.

Zhao, G. and Gao, H.: Automatic Correction of Contaminated Images for Assessment of Reservoir Surface Area Dynamics, Geophys. Res. Lett., 45, 6092–6099, https://doi.org/10.1029/2018GL078343, 2018.

Zhao, G., Bates, P., and Neal, J.: The Impact of Dams on Design Floods in the Conterminous US, Water Resour. Res., 56, e2019WR025380, https://doi.org/10.1029/2019WR025380, 2020.

Zheng, Y., Liu, P., Cheng, L., Xie, K., Lou, W., Li, X., Luo, X., Cheng, Q., Han, D., and Zhang, W.: Extracting operation behaviors of cascade reservoirs using physics-guided long-short term memory networks, J. Hydrol. Reg. Stud., 40, 101034, https://doi.org/10.1016/j.ejrh.2022.101034, 2022.

Zomer, R. J., Xu, J., and Trabucco, A.: Version 3 of the Global Aridity Index and Potential Evapotranspiration Database, Sci. Data, 9, 409, https://doi.org/10.1038/s41597-022-01493-1, 2022.